Dalton Transactions

Enhanced magneto-dielectric coupling in multiferroic Fe and Gd codoped PbTiO3 nanorods synthesized via microwave assisted technique

Journal:	*Dalton Transactions*
Manuscript ID:	DT-ART-02-2015-000638.R1
Article Type:	Paper
Date Submitted by the Author:	17-Apr-2015
Complete List of Authors:	Dutta, Dimple; BARC, Mandal, Balaji; Bhabha Atomic Research Centre, Chemistry Abdelhamid, Ehab; Wayne State University, Naik, Ratna; Wayne State University, Tyagi, A.; BARC, Chemistry

Enhanced magneto-dielectric coupling in multiferroic Fe and Gd codoped $PbTiO_3$ nanorods synthesized via microwave assisted technique

Dimple P. Dutta[a*], Balaji P. Mandal[a], E. Adb ElHamid[b], Ratna Naik[b] and Avesh K. Tyagi[a*],

[a] *Chemistry Division, Bhabha Atomic Research Centre, Mumbai 400085, India*
[b] *Department of Physics and Astronomy, Wayne State University, Detroit 48201, Michigan, United States*
email: dimpled@barc.gov.in; aktyagi@barc.gov.in

Abstract
The quest for new multiferroic materials is on the rise due to their potential applications in spintronics and futuristic multiple state memory devices. Here we report the microwave synthesis of iron/ gadolinium codoped $PbTiO_3$ nanorods which displays multiferroic behavior. Both the undoped and doped $PbTiO_3$ samples have been characterized using powder X-Ray diffraction, energy dispersive X-ray spectroscopy (EDS) and X-ray photoelectron spectroscopy (XPS) techniques. The morphology of the samples have been studied using transmission electron microscopy (TEM) and high resolution transmission electron microscopy (HRTEM) which confirmed the formation of nanorods. The substitution of Fe ions for Ti and Gd ions for Pb enhances the ferromagnetic and ferroelectric properties of this system. The reasons for this observation have been explored in detail. The ferroelectric, magnetic and magneto-capacitive measurements at room temperature substantiate the multiferroic nature of the codoped samples with significant magnetoelectric coupling observed in case of nano $PbTiO_3$:Gd^{3+}(0.5%):Fe^{3+}(5%).

Introduction

Research on multiferroics has gained a lot of prominence in the last two decades.[1-4] Generally, this class of materials exhibit coexistence of a number of order parameters (ferroelectric and magnetic) and their mutual coupling can lead to the development of futuristic multifunctional devices.[5,6] Multiferroic materials have immense potential applications in multiple state memory, spintronics, transducers and electronic field controlled ferromagnetic resonance devices.[7-9] The natural occurrence of such materials is a rarity since cation off-centering in ferroelectrics requires formally empty d-orbitals whereas partially filled d-orbitals are needed for the presence of magnetism. The simultaneous existence of these two contra-indicating factors in a single material is possible if the off-centred atom is different from that responsible for the magnetic moment. Multiferroicity has been reported in $BiFeO_3$ and $BiMnO_3$ where ferroelectricity is due to the non-centrosymmetric Bi^{3+} ion whereas Mn^{3+} and Fe^{3+} ions account for the magnetism.[10-13] However, these materials report low coupling between the ferroelectric and magnetic orders and

generally a large magnetoelectric effect at room temperature is required for various device applications such as spintronics, data-storage media, and multiple-state memories.[14,15] Hence, there is a continuous quest for new materials that can exhibit multiferroicity along with promising magnetoelectric/ magnetodielectric /magnetocapacitance effects in which the electric field/ dielectric permittivity /capacitance can be controlled by an applied magnetic field and vice versa.

A lot of interest has been generated in recent times on the realization of ferromagnetism in classic perovskite ferroelectric materials like $BaTiO_3$ via appropriate doping.[16,17] $PbTiO_3$ has been considered to be one of the most important members of the perovskite family due to its high Curie temperature, pyroelectric coefficient, spontaneous polarization and low dielectric constant.[18] The Ti^{4+} ions which have a d^0 configuration, distorts away from their ideal position in cubic symmetry and this results in the observed spontaneous polarization in $PbTiO_3$. Substituting a part of these Ti^{4+} ions with transition metal ions having partially filled d orbitals can lead to the development of ferromagnetism in the material. Recent reports on ferromagnetism observed in Fe doped $PbTiO_3$ is a testimony to this fact.[19] However, the ferromagnetism exhibited by these materials at room temperature is quite low and further improvement is needed for its ultimate application in magnetoelectric devices. An enhancement in the ferromagnetic properties of such oxide materials on downsizing them to the nanoscale has been theoretically predicted.[20,21] This has been attributed to the presence of oxygen vacancies on the surface of these nanoparticles. Consequently, multiferroicity has been reported in undoped $PbTiO_3$ nanoparticles synthesized via polymer precursor method.[22] Also Fe doped $PbTiO_3$ nanoparticles synthesized via surfactant assisted hydrothermal and sol gel techniques exhibited a slight improvement in ferromagnetism compared to the undoped nano $PbTiO_3$.[23,24]

Here we report the microwave assisted synthesis of undoped and Fe/Gd doped $PbTiO_3$ nanorods. In this synthesis technique, electric dipoles present in the solvent medium respond to the electric field resulting in the constant reorientation of the reactant molecules which leads to generation of heat due to friction.[25] The microwave assisted method is thus faster and energy efficient compared to conventional techniques for synthesis of nanomaterials.[26] The higher aspect ratios obtained for $PbTiO_3$ nanorod morphology compared to nanoparticles, can lead to its better

practical applications in memory devices and photonics.[27] Hence it was of interest to study the effect of nanorod morphology on the multiferroicity of $PbTiO_3$ doped with Fe^{3+} and Gd^{3+} ions. The choice of dopants was based on the fact that they are both magnetically active and the interactions between them can impart ferromagnetism in the ferroelectric $PbTiO_3$, rendering it a multiferroic nature.[28] The nanorods have been characterized using powder X-ray diffraction (XRD), energy dispersive X-ray spectroscopy (EDS) and X-ray photoelectron spectroscopy (XPS) techniques and their morphology have been studied using transmission electron microscopy (TEM) and high resolution transmission electron microscopy (HRTEM). The magnetic and ferroelectric properties of the above samples have been investigated from their *M-H* and *P-E* curves. Magneto-dielectric coupling experiments have been done to establish the multiferroic nature of these doped $PbTiO_3$ samples.

Results and Discussion

The powder XRD pattern recorded for the as prepared samples synthesized via microwave assisted technique indicated that they were amorphous in nature. On furnace heating at 500°C for 3h, highly crystalline $PbTiO_3$ samples were formed which could be verified from XRD. The XRD patterns of the thermally treated undoped as well as Fe doped $PbTiO_3$ samples are shown in Figure 1(a-d). The diffraction profile of all the samples could be indexed to tetragonal $PbTiO_3$ with space group *P4mm* (PCPDF file 772002). With increase in Fe doping, a decrease in the tetragonal distortion is observed as inferred by the gradually decreasing resolution of the doublet at 2θ between 32 to 34°. The position of the (100) peak shifts gradually to lower angle which indicates an increase in the lattice parameters. This can be attributed to the doping of Fe^{3+} ions in the Ti^{4+} ion sites in the $PbTiO_3$ lattice since the former has a larger radius (0.64Å) and different electron density compared to the latter (0.60Å) in octahedral coordination number.[23] Phase pure $PbTiO_3$ samples with upto 5mol% Fe doping have been obtained using our microwave assisted technique which is in contrast to that reported in case of surfactant assisted as well as coprecipitation synthesis which always yielded $Pb_2Ti_2O_6$ as an impurity phase.[24,29] On doping $PbTiO_3$ with Gd^{3+} ions, interesting observations were noted from the powder XRD pattern (Figure 2a-d) of the thermally treated samples. For 0.5mol% Gd^{3+} doping, the diffraction peaks suggested the formation of phase pure tetragonal $PbTiO_3$ having space group *P4mm* (PCPDF file 772002) which is similar to that observed in case of Fe doping. The slight shifting of the

diffraction peaks to higher angles and consequent lattice contraction can be explained on the basis of smaller ionic radius of Gd^{3+} (0.94Å) compared to Pb^{2+} (1.19Å) and also on presence of Pb vacancies. In case of $PbTiO_3$:Gd^{3+}(2%) sample, the powder XRD pattern indicated formation of minute amount of $PbTi_3O_7$ as an additional phase. Further increase in Gd^{3+} doping to 5mol% resulted in the formation of predominantly monoclinic $PbTi_3O_7$ with space group $P2_1$ (PCPDF file 701016) and a minor fraction of tetragonal $PbTiO_3$. The increase in the Pb deficient $PbTi_3O_7$ phase with increase in Gd^{3+} doping is an indication of its lower dopant solubility. Similar observations have been reported in case of Er^{3+} doped $PbTiO_3$.[30] $PbTiO_3$ belongs to the perovskite family which ideally has a cubic closed packed anion sub-lattice structure. This lattice is unable to accommodate the large excess of oxygen which is inevitable with donor doping like Gd^{3+} ions. Hence, with increase in Gd^{3+} ions in the reaction mixture, a titanium rich phase $PbTi_3O_7$ is predominantly obtained as the major product, which is due to an anion-excess induced phase separation of the perovskite lattice. The powder XRD patterns of the Fe/Gd codoped $PbTiO_3$:Gd^{3+}(0.5%):Fe^{3+}(2%), $PbTiO_3$:Gd^{3+}(0.5%):Fe^{3+}(5%) and $PbTiO_3$:Gd^{3+}(2%):Fe^{3+}(2%) samples are shown in Figure 3a-c. The diffraction peaks for $PbTiO_3$:Gd^{3+}(0.5%):Fe^{3+}(2%) and $PbTiO_3$:Gd^{3+}(0.5%):Fe^{3+}(5%) could be indexed to tetragonal $PbTiO_3$ with lattice constants a = 3.89Å, c = 4.12Å and a = 3.88Å, c = 4.09Å, respectively. It can be clearly seen that with increase in Gd^{3+} doping to 2mol% in the Fe/Gd codoped sample, monoclinic phase of $PbTi_3O_7$ is obtained as the sole product (PCPDF 701016).

The compositions of the undoped and single as well as codoped $PbTiO_3$ samples have been further analysed using XPS spectra. The representative XPS survey spectra for a few samples have been shown in Figure 4. The C1s peak seen in all the spectra is due to the deposition of the samples on carbon tape. The XPS spectrum of undoped $PbTiO_3$ (Figure 4a) shows the presence of only Pb, Ti and O in the sample. The $Pb4f_{7/2}$ and $Pb4f_{5/2}$ binding energy peaks at 137.23 and 142.3eV, respectively, are separated by ~ 5.07eV which is similar to that reported in case of $PbTiO_3$ nanostrips.[31] For the Ti 2p core levels, the $2p_{3/2}$ (458.46eV) and $2p_{1/2}$ (464.13eV) doublet exhibits an energy gap of 5.67eV which is comparable to that reported for ceramic $PbTiO_3$ [32]. The O1s peak at 530.9eV corresponds to the Ti-O lattice oxygen in our undoped $PbTiO_3$ sample. For $PbTiO_3$:Fe^{3+}(5%), the XPS survey spectrum (Figure 4b) confirmed the presence of Fe^{3+} ions with the binding energies of Fe^{3+} $2p_{3/2}$ and $2p_{1/2}$ spin orbit doublets at 711.2 and 724.5eV, respectively. These values are slightly more than that reported for Fe_2O_3 which is

710.7 eV for $2p_{3/2}$ and 724.3 eV for $2p_{1/2}$.[32] The $Ti2p_{3/2}$ and $Ti2p_{1/2}$ peaks are seen at lower binding energy (457.7eV and 463.7eV, respectively) compared to undoped $PbTiO_3$. This suggests the substitution of Ti^{4+} in $PbTiO_3$ lattice with Fe^{3+} ions and can be attributed to the large concentration of oxygen vacancies.[33] The transfer of electrons from Fe^{3+} to Ti^{4+} is also manifested in the broadness of the $Ti2p_{3/2}$ and $Ti2p_{1/}$peaks in the Fe doped samples, which is due to the presence of the Ti ions in various oxidation states. The XPS survey spectrum of $PbTiO_3$:Gd^{3+}(0.5%) (Figure 4c) shows the presence of Gd 4d core level binding energy peak at 146.18eV. The codoped $PbTiO_3$:Gd^{3+}(0.5%):Fe^{3+}(5%) sample exhibited binding energy peaks corresponding to all the constituent elements i.e. Pb, Ti, Fe, Gd and O (Figure 4d).

The core level O 1s XPS spectra for the undoped as well as single and Fe/Gd codoped $PbTiO_3$ is shown in Figure 4e. All the doped samples exhibited two peaks with the major peak at a lower binding energy of ~530.7 – 531.5eV which corresponds to the lattice oxygen of $PbTiO_3$. The minor peak at ~ 533.5eV is due to hydroxyl group or adsorbed oxygen on the surface of the samples.[34] The minor peak is more pronounced in case of the Fe/Gd doped nano $PbTiO_3$ which suggests that there is an increase in the concentration of oxygen vacancies in these samples [33]. Compared to undoped $PbTiO_3$, the O1s peak shifts to lower binding energy in $PbTiO_3$:Fe^{3+}(5%) sample which can be explained on the basis of the partial substitution of Ti^{4+} with Fe^{3+} ions. The O1s binding energy in Ti-O(1s) bond is higher than that in Fe-O(1s) bond and hence a slight decrease in binding energy is observed in case of the Fe doped sample.[35]

The size, morphology and composition of the undoped and Fe/Gd doped $PbTiO_3$ samples have been also determined using TEM, HRTEM and EDS techniques. An idea about the dimensions of the undoped $PbTiO_3$ and $PbTiO_3$:Fe(5%) nanorods has been obtained from the TEM images (Figure 5a and 5f). For the undoped $PbTiO_3$ samples, the length of the nanorods range between 100-200nm, whereas for the Fe doped sample, it is between 80-120nm. The diameter of the nanorods increases slightly from ~ 15 – 20nm in case of undoped $PbTiO_3$ to ~ 25 – 30nm for the $PbTiO_3$:Fe(5%) sample. In soft chemical synthesis of nanomaterials, the morphology of the product obtained depends on various parameters like growth conditions, precursor type and concentration, etc.[36] In our experiment, the introduction of the dopant Fe ion in the $PbTiO_3$ matrix, leads to an alteration in the dimension of the nanorods. From the XRD patterns of the undoped and Fe doped samples (Figure 1), it can be seen that there is a preferential orientation of

the nanorods along the [101] direction and the tetragonality of the structure decreases with increase in Fe doping. The lattice constants obtained for our undoped $PbTiO_3$ are a = 3.897Å and c = 4.151Å, which is similar to that reported for $PbTiO_3$ nanostrips.[31] With increase in Fe doping, a decrease in *c* parameter and slight increase in *a* parameter is observed. For the $PbTiO_3$:Fe(5%) sample, the lattice constants were found to be a = 3.926Å and c = 4.068Å, which decreases the tetragonal ratio (c/a) from 1.065 in undoped to 1.036 in 5% Fe doped $PbTiO_3$. This indicates that with the doping of Fe in $PbTiO_3$, the growth along the c axis is mostly affected. As Fe^{3+} ions replace Ti^{4+} ion sites in the lattice, there might be an alteration in the positive charge concentration along the c direction and there is probability of defects being introduced in the crystal structure. These factors reduce the surface energy which ultimately hinders growth along one direction and reduces the length of the nanorods.[37] The EDS spectra (Figure 5b and 5d) confirms the presence of Pb, Ti, O in both samples and also Fe in $PbTiO_3$:Fe(5%). In undoped $PbTiO_3$, the atomic ratio of Pb to Ti to O is found to be 1.025 : 1.000 : 2.975. Spectra taken at a number of selected positions of the sample confirm the presence of the same constituents. The HRTEM images of undoped and 5% Fe doped $PbTiO_3$ nanorods are shown in Figures 5e and 5f, respectively. The micrograph of both samples shows clear crystal domain with uniform interplanar spacing of ~0.284 nm, corresponding to the (1 0 1) plane. The corresponding SAED patterns (shown as inset of Figures 5e and 5f) are regular, and can be indexed as the incident electron beam parallel along the [101] direction.

The magnetic properties of the undoped and Fe/Gd doped nano $PbTiO_3$ samples have been investigated by studying the magnetization variation as a function of applied field at room temperature (300K). The *M-H* curves obtained for all the samples after diamagnetism correction is shown in Figure 6 and corresponding saturation magnetization (M_s) and coercivity (H_c) values have been given in Table 1. For all the samples we can observe sizable hysteresis with a finite value of the coercive field. Bulk pure $PbTiO_3$ is an intrinsic diamagnetic compound. However, very mild room temperature ferromagnetism has been reported for $PbTiO_3$ nanoparticles which has been attributed to the size effect and presence of oxygen vacancies.[23,38] The $PbTiO_3$ nanorods synthesized by us using microwave assisted technique shows a *S*-type hysteresis curve with a M_s value of 0.013 emu/g which is approximately three times higher than that observed for $PbTiO_3$ nanoparticles synthesized using sol gel technique (0.0041 emu/g).[38] This is due to the fact that specific surface area which is a critical factor for the observation of different properties in

nanomaterials, is higher in case of nanorods compared to nanospheres, for a given volume.[39] Hence the extent of surface defect concentration, which is the prime driving force for the observed ferromagnetism in nano $PbTiO_3$, will be higher in case of nanorod morphology. An increase in the M_s values is observed in case of Fe doped $PbTiO_3$ samples (Table 1). This has been attributed to the F-center exchange mechanism where electrons trapped in oxygen vacancies (*F* center) created by Fe^{3+} doping in Ti^{4+} sites in $PbTiO_3$ plays a major role.[23] It has been theoretically proved that, in $PbTiO_3$, the electron occupies an orbital which overlaps with the adjacent iron d orbitals forming Fe^{3+}–V_O^{2-}–Fe^{3+} groups.[40] The F center act as bound magnetic polaron and its exchange interaction with iron leads to the observed ferromagnetic coupling. The M_s values for our $PbTiO_3$:Fe(5%) sample (0.453emu/g) is higher than that reported for hydrothermally synthesized $PbTiO_3$:Fe(4%) nanoparticles (0.008 emu/g) and $PbTiO_3$:Fe(1%) nanocrystals (0.075 emu/g) having self-assembled disk-like superstructures.[23,41] This may be due to the formation of larger number of oxygen vacancies in our Fe doped $PbTiO_3$ samples synthesized using the microwave assisted technique. Similar observations have been reported for microwave-synthesized homogeneous $Ce_{0.5}Zr_{0.5}O_2$ solid solution where more zirconia was incorporated into the ceria lattice and higher surface defective sites were formed in the sample compared to that prepared using coprecipitation method.[42]

Room temperature ferromagnetism has also been observed in case of the $PbTiO_3$:Gd(0.5%) sample, which exhibits a M_s value of 0.020 emu/g (Table 1). From our powder XRD results, it is clear that the rare earth Gd^{3+} ion substitutes Pb^{2+} ions of $PbTiO_3$ at the A site. Hence, it acts as a donor where lead vacancies created in distant coordination spheres of $PbTiO_3$ takes care of the charge compensation.[43] Compared to $PbTiO_3$:Fe(0.5%), the $PbTiO_3$:Gd(0.5%) sample is thus expected to have lesser number of oxygen vacancies but higher number of lead vacancies.[43] The observed ferromagnetism in this $PbTiO_3$:Gd(0.5%) sample is induced by the oxygen vacancies and mainly originates from the spin-polarized d_{zx} and d_{x2-y2} states of the two nearest Ti atoms.[44]

The *M-H* curves obtained for Fe/Gd codoped $PbTiO_3$ samples shows interesting results. The M_s as well as H_c values for the $PbTiO_3$:Gd(0.5%)Fe(2%) and $PbTiO_3$:Gd(0.5%)Fe(5%) samples are less than that observed in case of single doped $PbTiO_3$:Fe(2%) and $PbTiO_3$:Fe(5%) samples, respectively (Table1). It has been well established that Fe^{3+} acceptor doping in Ti^{4+} sites in $PbTiO_3$ leads to the formation of oxygen vacancies which promote ferromagnetism by the exchange interaction between two irons via *F* center.[23] In case of the $PbTiO_3$:Gd(0.5%)Fe(5%)

sample, the Gd^{3+} donor doping in Pb^{2+} site leads to formation of lead vacancies in distant coordination spheres.[43] Hence, there is a possibility of net reduction in oxygen vacancies which plays a major role in the observed ferromagnetic behavior of these samples. For $PbTiO_3$:Fe(2%), $PbTiO_3$:Fe(5%), $PbTiO_3$:Gd(0.5%)Fe(2%) and $PbTiO_3$:Gd(0.5%)Fe(5%) samples, a slight linearization of the *M-H* curve is observed which indicates the presence of paramagnetic component in the system. Both Fe^{3+} and Gd^{3+} are paramagnetic ions and can give rise to Fe^{3+}–O–Fe^{3+} / Gd^{3+}–O–Gd^{3+} superexchange interaction with oxygen ions which are antiferromagnetic in nature. Hence, the appearance of the linear variation in the *M-H* curves for all the $PbTiO_3$ samples with ≥ 2mol% doping of Fe/Gd ions can be attributed to the contributions from these paramagnetic/antiferromagnetic components.[23]

From Table 1, it is evident that the highest M_s values at room temperature has been observed in case of the $PbTiO_3$:Fe(5%), $PbTiO_3$:Gd(0.5%)Fe(5%) and $PbTiO_3$:Fe(2%) samples. The temperature dependence of magnetization studies at an applied field of 500Oe has been done on these samples to determine the nature of magnetic ordering and the resulting plots are shown in Figure 7a-c. Between ~150 to 300K, constant magnetization values of 0.14 emu/g, 0.12 emu/g, and 0.04 emu/g have been obtained for the $PbTiO_3$:Fe(5%), $PbTiO_3$:Gd(0.5%)Fe(5%) and $PbTiO_3$:Fe(2%) samples, respectively. The results suggest the retention of long range magnetic ordering in the samples at room temperature.[23] At temperatures lower than 150K, the rapid increase in the magnetization values indicates the presence of frozen isolated Fe^{3+} ions in the host $PbTiO_3$ matrix that contribute to the paramagnetic component. The *M* vs *H* plots at two different temperatures (50K and 300K) for these three samples are shown as inset in Figure 7a-c. In case of the low temperature *M-H* curves recorded at 50K, the linear component increases indicating that paramagnetic contribution is quite dominant in the low temperature range. From the M vs H curves obtained at 50K and 300K we have plotted M/M_s (M_s is the saturation magnetization) vs H/T for our $PbTiO_3$:Fe(5%), $PbTiO_3$:Gd(0.5%)Fe(5%) and $PbTiO_3$:Fe(2%) samples (supplementary Figure S1). It is observed that the curves remain distinct which rules out the possibility of presence of superparamagnetism, since it is well known that the curves merge into a single one for superparamagnetic systems. [45]

The room temperature electric polarization versus electric field (*P-E*) measurements has been recorded for the undoped and Gd/Fe doped $PbTiO_3$ samples at a frequency of 1kHz. Bulk $PbTiO_3$ is a well studied displacive type ferroelectric material and the *P-E* curves of all our nano

$PbTiO_3$ samples exhibit the distinctive hysteresis loop as is evident from Figure 8a. It is evident that these materials are somewhat lossy, which is a common observation for polycrystalline materials. The coercive field (E_c), remnant polarization (P_r) and spontaneous polarization (P_s) values estimated from the room temperature *P–E* hysteresis loops of all the samples are listed in Table 2. The ferroelectric distortion in $PbTiO_3$ is stabilized via Ti(3d)–O(2p) hybridization which results in the displacement of the Ti^{4+} ions with respect to the oxygen octahedral cage.[46] As mentioned before, subtituting Ti^{4+} ions with Fe^{3+} in our sonochemically synthesized $PbTiO_3$ samples, the tetragonal distortion (*c/a*) reduces from 1.065 in undoped $PbTiO_3$ to 1.036 in 5% Fe doped $PbTiO_3$. Inspite of the decrease, the extent of distortion is still high enough to sustain ferroelectric behavior in Fe doped $PbTiO_3$. This is reflected in the P_s, P_r and coercivity (E_c) values obtained for our $PbTiO_3$:Fe(0.5%), $PbTiO_3$:Fe(2%) and $PbTiO_3$:Fe(5%) samples (Table 2). Generally, acceptor doping in perovskites as well as reduced tetragonality, leads to lower electric polarization values and higher cooercivity.[47] However in our case, compared to undoped $PbTiO_3$, an increase in the P_s, P_r and E_c values have been observed in all the Fe doped $PbTiO_3$ samples. This increase in the P_s and P_r values should be extrinsic in nature and may arise due to the space charge effect. Similar observations have been reported for Cu doped $K_{0.5}Na_{0.5}NbO_3$ ceramics.[48] With increase in Fe doping from 2 to 5 mol%, a slight decrease in the P_s and P_r values have been observed. This can be explained on the basis of presence of larger number of oxygen vacancies in the latter. This leads to a stronger pinning effect with lower ferroelectric domain switching under an electric field which results in a decrease in the P_r value.[49]

In case of $PbTiO_3$:Gd(0.5%), a slight increase in the P_s and P_r values have been observed compared to undoped $PbTiO_3$. As Gd^{3+} gets substituted in the Pb^{2+} sites of $PbTiO_3$, it can be regarded as a donor dopant and hence results in the formation of cation vacancies by the following reaction

$$Gd^{3+} \longrightarrow Gd^{\bullet}_{Pb} + xV''_{Pb} + yV''''_{Ti} \quad (2x + 4y = 1) \qquad (1)$$

These cation vacancies generated by donor doping makes domain motion easier and enhance the ferroelectric properties resulting in enhanced P_s and P_r values.[50] For the Fe/Gd codoped $PbTiO_3$: Gd^{3+}(0.5%)Fe^{3+}(2%) and $PbTiO_3$: Gd^{3+}(0.5%)Fe^{3+}(5%) samples, the P_s and P_r values obtained are less than that of the corresponding single doped $PbTiO_3$:Fe(2%) and $PbTiO_3$:Fe(5%) (Table 2). In case of double doping, Gd^{3+} acts as donor dopant whereas Fe^{3+} act as acceptor dopant at the Pb^{2+} and Ti^{4+} sites of $PbTiO_3$, respectively. Substitution of Fe^{3+} on Ti^{4+} sites is compensated

by the creation of oxygen vacancies and/or the annihilation of cation vacancies, as shown by the following reactions[51]

$$Fe_2O_3 \longrightarrow 2Fe'_{Ti} + 3O_o + V^{\bullet\bullet}_o \quad (2)$$

$$Fe^{3+} + xV''_{Pb} + yV''''_{Ti} \longrightarrow Fe'_{Ti} \quad (2x + 4y = 1) \quad (3)$$

Hence, compared to the Fe single doped samples, there will be less concentration of oxygen vacancies in the Fe/Gd double doped samples which reduces the pinning effect on the domain walls, leading to enhanced remnant polarization and lower coercive field. Hence, by careful optimization of the dopant concentrations, it is possible to have $PbTiO_3$ nanomaterials that can exhibit multifunctionality through extrinsic manipulations.

In order to understand the effects of the oxygen and Pb ion vacancies, the leakage currents for all the samples have been measured, and the results obtained have been shown in Figure 8b. Higher values of leakage current compared to undoped $PbTiO_3$ have been observed for our Fe doped $PbTiO_3$ samples synthesized via microwave assisted technique and the magnitude of leakage current increases with increased amount of Fe doping. Fe^{3+} has a lower valence than Ti^{4+} and hence plays the role of an acceptor which leads to formation of oxygen vacancies. The neutralized oxygen vacancies releases one or two electrons under the application of an electric field and gets ionized. The weak bond between these conduction electrons with oxygen vacancies has been reported to act as shallow electron traps.[52] This provides a comparatively lower energy path for conduction by facilitating localized electron transport between neighboring transition metals via hopping through oxygen vacancies which increases the leakage current.[53] Hence, leakage current densities of 0.65μA/cm^2, 1.50μA/cm^2 and 2.12μA/cm^2 have been obtained for our $PbTiO_3$:Fe(0.5%), $PbTiO_3$:Fe(2%) and $PbTiO_3$:Fe(5%) samples, respectively, under an applied electric field of ~7kV/cm. A marked decrease in the leakage current density compared to single doped $PbTiO_3$:Fe(2%) and $PbTiO_3$:Fe(5%) has been observed for the Fe/Gd double doped $PbTiO_3$:Gd(0.5%)Fe(2%) and $PbTiO_3$:Gd(0.5%)Fe(5%) samples. This is due to the reduced concentration of oxygen vacancies in the Fe/Gd double doped $PbTiO_3$ which leads to the less leaky P-E hysteresis loops exhibited by them compared to the corresponding Fe single doped $PbTiO_3$ samples.

The $PbTiO_3$:Fe(2%), $PbTiO_3$:Fe(5%), $PbTiO_3$:Gd(0.5%)Fe(2%) and $PbTiO_3$:Gd(0.5%)Fe(5%) samples exhibit ferromagnetism as well as ferroelectricity at room temperature. The best results have been obtained for $PbTiO_3$:Gd(0.5%)Fe(5%) which shows M_s 0.385emu/g, P_s 0.464μC/cm^2

and Pr 0.195μC/cm^2 with less leaky features compared to the single doped $PbTiO_3$:Fe(5%) sample. Hence there is a probability of observing magnetocapacitive coupling in these samples which is a true indicator of the extent of multiferroicity present in them and their possible application in multistate data storage devices and magnetically tunable high frequency electronic devices. The induction of magnetization with the application of an electric field or the induction of a polarization with the application of a magnetic field signifies magnetoelectric coupling in the sample.[54] The magnetic field dependence of capacitance for our $PbTiO_3$:Fe(5%) and $PbTiO_3$:Gd(0.5%)Fe(5%) samples have been measured and the corresponding room temperature magnetocapacitance measured at 30kHz is shown in Figure 9a and 9b, respectively. The magnetic field induced magnetocapacitive shift is ~0.046% and 0.021% in an applied field of 10kOe for the $PbTiO_3$:Gd(0.5%)Fe(5%) and $PbTiO_3$:Fe(5%) samples, respectively. The magnetocapacitive effect originates from scalar P^2M^2 terms present in the Ginzburg–Landau free energy expansion equation.[11] Such quadratic dependence of dielectric constant and magnetization has been reported for $EuTiO_3$, $BiMnO_3$, etc.[55] This second order dependence is amply reflected in the magnetocapacitance coupling exhibited by both the samples. A partial shift towards linear dependence is observed in the magnetocapacitance coupling in case of the double doped $PbTiO_3$:Gd(0.5%)Fe(5%) sample (Figure 9a). This might be due to an additional term proportional to P^2M in the free energy, or could also result from a linear magnetoelectric coupling producing a modification in the bi-quadratic P^2M^2 free energy term.

Conclusion

In summary, undoped as well as Fe/Gd single and double doped $PbTiO_3$ nanorods have been synthesized successfully using a facile microwave assisted technique. From powder XRD patterns it was established that phase pure $PbTiO_3$ samples with upto 5mol% Fe doping and 0.5% Gd doping could be obtained via this method of synthesis. A decrease in the tetragonal distortion of $PbTiO_3$ was observed with increase in Fe doping. The compositions of the samples have been confirmed using XPS and EDS. From TEM micrographs a decrease in the length of the $PbTiO_3$ nanorods was observed with increased doping of Fe/Gd ions. The $PbTiO_3$ nanorods exhibit mild room temperature ferromagnetism in contrast to that that observed in case of bulk $PbTiO_3$ which is diamagnetic. The addition of Fe/Gd dopants in varying amounts alters the magnetic as well as the ferroelectric properties of the $PbTiO_3$ samples. This has been attributed to the presence of

oxygen and Pb vacancies. The best results have been obtained for the $PbTiO_3$:Gd(0.5%)Fe(5%) sample which exhibits a M_s value of 0.385 emu/g and P_s of 0.464μC/cm^2 with considerably less leaky characteristics compared to the single doped $PbTiO_3$:Fe(5%). Magnetoelectric coupling in these $PbTiO_3$:Gd(0.5%)Fe(5%) nanorods have also been established by magnetocapacitance measurements which suggest possible tunability of the dielectric constant with external magnetic field.

Experimental Section

Each experiment was carried out under ambient conditions at room temperature (27°C). AR grade lead nitrate [$Pb(NO_3)_2$], titanium isopropoxide [$Ti(OPr^i)_4$], ferric nitrate [$Fe(NO_3)_3.9H_2O$] and gadolinium nitrate [$Gd(NO_3)_3.6H_2O$] were procured from commercial sources.

Synthesis of undoped $PbTiO_3$

To an aqueous suspension of $Ti(OPr^i)_4$ (2.196g, 7.73mmol) in deionized water, an aqueous solution of $Pb(NO_3)_2$ (2.561g, 7.73mmol) was added. The pH of the solution was adjusted to ~ 11 by adding ammonia solution. The resultant mixture was transferred to a 250ml round bottom flask fitted with a condenser attachment and exposed to microwave irradiation (MicroSYNTH, 500W, 2.45 GHz frequency multimode source) for 15min. The milky white colloidal suspension was centrifuged at 500rpm for 3min. The precipitate was washed with distilled water and ethanol and dried in air. The dried product was furnace heated at 500°C for 3h.

Synthesis of Fe/Gd doped $PbTiO_3$

The method reported above was followed but with the addition of stoichiometric amounts of the salts of the metal ions to be doped in the $PbTiO_3$ sample. Thus single doped $PbTiO_3$:M(x%) (M= Fe^{3+}, Gd^{3+}; x = 0.5, 2 and 5) and Fe/Gd codoped $PbTiO_3$ samples have been synthesized using this method.

Characterization

The powder XRD patterns of the samples were recorded on a PANalytical X-Pert Pro powder x-ray diffractometer in the 2θ range 10°–80° using CuK_α (k = 1.5406 and 1.5444Å) radiation. The

samples were mixed with collodion binder and smeared on glass plates. EDX analyses were done using an Inca Energy 250 instrument. Conventional TEM micrographs were recorded on a Libra 120 KeV Electron Microscope (Carl Zeiss). The samples were dispersed in ethanol and deposited on carbon coated copper grids. X-ray photoelectron spectra (XPS) were recorded on VG Microtech FISON instrument using Mg-Kα radiation (1253.6eV). The field dependent magnetic measurements at room temperature were carried out using Quantum Design Physical Properties Measurement System (PPMS). Magnetic field-dependent dielectric measurements were performed using Agilent 4284A LCR meter while the magnetic field was controlled by the above mentioned PPMS instrument. For the magnetocapacitive measurements, both the sides of the pellets were coated with silver epoxy and Au wires were attached to make a parallel plate capacitor. The magnetocapacitance data was obtained after performing the background correction. For *P-E* measurements, the samples were pelletized and coated with Pt paste and the ferroelectric studies were done on aixACCT TF Analyzer 2000 FE at 1 to 20 kHz ac frequency. The leakage currents on these samples were also measured on the same instrument.

Acknowledgement

The Department of Atomic Energy's Science Research Council (DAE-SRC) is acknowledged for supporting this work via sanction number 2010/21/9-BRNS/2025 dated 7-12-2010.

References

1. H. Schmid, *Ferroelectrics,* 1994, **162,** 317–338.
2. N. Hur, S. Park, P. A. Sharma, J. S. Ahn, S. Guha and S-W. Cheong, *Nature,* 2004, **429,** 392–395.
3. Y. Yamasaki, S. Miyasaka, **Y**. Kaneko, J.-P. He, T. Arima, and **Y**. Tokura, *Phys. Rev. Lett.,* 2006, **96,** 207204.
4. M. Mostovoy, *Phys. Rev. Lett.,* 2006, **96,** 067601.
5. S-W. Cheong and M. Mostovoy, *Nature Mater*., 2007, **6**, 13-20.
6. R. Ramesh and N. A. Spaldin, *Nature Mater*., 2007, **6**, 21-29.
7. J. Wang, J. B. Neaton, H. Zheng, V. Nagarajan, S.B. Ogale, B. Liu, D. Viehland, V. Vaithyanathan, D. G. Schlom, U. V. Waghmare, N. A. Spaldin, K. M. Rabe, M. Wuttig and R. Ramesh, *Science,* 2003, **299**, 1719-1722.
8. M. Fiebig, T. Lottermoser, D. Fro¨hlich, A.V. Goltsev and R.V. Pisarev, *Nature*, 2002, **419**, 818-820.
9. T. Kanai, S. I. Ohkoshi, A. Nakajima, T. Watanabe and K. Hashimoto, *Adv. Mater*, 2001, **13**, 487-490.
10. D. P. Dutta, B. P. Mandal, M.D. Mukadam, S.M. Yusuf and A. K. Tyagi, *Dalton Trans*., 2014, **43**, 7838 – 7846
11. D. P. Dutta, Balaji P. Mandal, Ratna Naik, Gavin Lawes and A. K. Tyagi, *J. Phys. Chem. C*, 2013, **117**, 2382-2389.
12. D. P. Dutta, O. D. Jayakumar, A. K. Tyagi, K.G. Girija, C. G. S. Pillai, and G. Sharma, *Nanoscale*, 2010, **2**, 1149-1154.
13. T. Kimura, S. Kawamoto, I. Yamada, M. Azuma, M. Takano, and Y. Tokura, *Phys. Rev. B,* 2003, **67**, 180401.
14. J. M. D. Coey, A. P. Douvalis, C. B. Fitzgerald, and M. Venkatesan, *Appl. Phys. Lett*., 2004, **84**, 1332.
15. M. Fiebig, T. Lottermoser, D. Frohlich, A. V. Golsev, and R. V. Pisarev, *Nature London* 2002, **419**, 819.
16. N. Apostolova, A. T. Apostolov, S. G.Bahoosh, and J. M. Wesselinowa, *J. Appl. Phys.,* 2013, **113**, 203904.
17. J. Shah and R. K. Kotnala, *J. Mater. Chem. A*, 2013, **1**, 8601–8608
18. Y. Chan, H. L. W. Chan, and C. L. Choy*, J. Am. Ceram. Soc*., 1998, **81**, 1231-1236.
19. V. R. Palkar and S. K. Malik, *Solid State Commun.,*. 2005, **134**, 783.
20. A. Sundaresan and C. N. R. Rao, *Nano Today*, 2009, **4**, 96–106.
21. Y. F. Zhukovskii, E. A. Kotomin, S. Piskunov, and D. E. Ellis, *Solid State Commun.,* 2009, **149**, 1359–1362.
22. M. Wang, Guo-L. Tan,w and Q. Zhang, *J. Am. Ceram. Soc*., 2010, **93**, 2151–2154.
23. Z. Ren, G. Xu, X. Wei, Y. Liu, X. Hou, P. Du, W. Weng, G. Shen, and G. Han, *Appl. Phys. Lett.,* 2007, **91**, 063106.
24. K. C. Verma, R. K. Kotnala, and N. S. Negi, *Appl. Phys. Lett*., 2008, **92**, 152902.
25. O. Palchik, J. Zhu and A. Gedanken, *J. Mater. Chem*., 2000, **10**, 1251-1254.
26. F. K. Liu, Pei-W. Huang, Yu-C. Chang, Fu-H. Ko and Tieh-C. Chu, *J. Mater. Res*., 2004, **19**, 469-473.

27. R. Sæterli, P. M. Rørvik, C. C. You, R. Holmestad, T. Tybell, T. Grande, A. T. J. van Helvoort and Mari-A. Einarsrud, *J. Appl. Phys*., 2010, **108**, 124320.
28. R. Guo, L. Fang, W. Dong, F. Zheng, and M. Shen, *J. Phys. Chem. C,* 2010, **114***,* 21390–21396.
29. V. R. Palkar and S. K. Malik, *Solid State Commun*., 2005, **134**, 783.
30. E.C. Paris, M.F.C. Gurgel, T.M. Boschi, M.R. Joya, P.S. Pizani, A.G. Souza, E.R. Leite, J.A. Varela and E. Longo, *J. Alloys and Compds*., 2008, **462**, 157–163.
31. H. Deng, Y. Qiu and S. Yang, *J. Mater. Chem.,* 2009, **19**, 976–982.
32. J. N. Kim, K. S. Shin, B. O. Park, J. H. Lee, N. K. Kim and S. H. Cho, *Smart Mater. Struct.*, 2003, **565**, 12.
33. B. Santara, P. K. Giri, S. Dhara, K. Imakita and M. Fujii, *J. Phys. D: Appl. Phys*., 2014, **47**, 235304 (14pp)
34. Y. Yang, X. Wang, C. Sun and L. Li, *J. Am. Ceram. Soc*., 2008, **91**, 3820–3822.
35. J. F. Moulder, W. F. Stickle, P. E. Sobol and K. D. Bomben, 1992 *Handbook of X-ray photoelectron spectroscopy*. Perkin-Elmer Corporation, Minnesota
36. M. Meshki, M. Behpour and S. Masoum, *J. Electroanal. Chem*., 2015, **740**, 1-7.
37. Z. Y. Tang, N. A. Kotov and M. Giersig, *Science,* 2002, **297**, 237-240.
38. Z. Zhang, J. Hua, Z. Xu, H. Qin, L.Sun, F. Gao, Y. Zhang and M. Jiang, *Solid State Sci*., 2011, **13**, 1391-1395.
39. W-N. Li, V. M. B. Crisostomo, E. K. Nyutu, Y-S. Ding and S. L. Suib, "*Nanorods, Nanotubes, and Nanomaterials Research Progress*," ed: Wesley V. Prescott, Arnold I. Schwartz, 2008, Nova Science Publishers, 227-228.
40. H. Meštric, R. A. Eichel, T. Kloss, K. P. Dinse, S. Lanbach, P. C. Schmidt, K. A. Schönau, M. Knapp, and H. Ehrenberg, *Phys. Rev. B,* 2005, **71**, 134109.
41. Z. Liu, Z. Ren, X. Wei, Z. Xiao, X. Hou, G. Shen, G. Xu, and G. Han, *J. Am. Ceram. Soc.*, 2010, **93**, 3610–3613.
42. B. M. Reddy, G. K. Reddy, I. Ganesh and J. M. F. Ferreira, *Catal. Lett.* 2009, **130**, 227–234
43. E. Erdem, P. Jakes, S.K.S. Parashar, K. Kiraz, M. Somer, A. Rüdiger and R-A. Eichel, *J. Phys.: Condens. Matter,* 2010, **22**, 345901 (7pp)
44. T. Shimada, Y. Uratani and T. Kitamura, *Acta Mater*., 2012, **60**, 6322-6330.
45. D. Karmakar, S.K. Mandal, R.M. Kadam, P.L. Paulose, A.K. Rajarajan, T.K. Nath, A.K. Das, I. Dasgupta, G.P. Das, *Phys. Rev. B* 2007, **75**,144404
46. R.E. Cohen and H. Krakauer, *Ferroelectrics,* 1992, **136**, 95.
47. H. We and, Y. Chen, 2014, doi.org/10.1016/j.ceramint.02.113
48. S. M. Ke, H. T. Huang, H. Q. Fan, H. K. Lee, L. M. Zhou, and Y.-W. Mai, *Appl. Phys. Lett.* 2012, **101**, 082901.
49. L. Wang, T. K. Song, S. C. Lee, J. H. Cho, Y. S. Sung, M. H. Kim and K. S. Choi, *Curr. Appl. Phys*. 2010, **10**, 1059.
50. S. Takahashi and M. Takahashi, *Jpn. J. Appl. Phys*., 1972, **11**, 31.
51. A. J. Moulson and J. M. Herber, *Electroceramics,* Wiley, Chichester, England, 2003, 313–315.
52. H. Ihrig and D. Hennings*, Phys. Rev. B* 1978, **17**, 4593.
53. M.H.R. Lankhorst, H.J.M. Bouwmeester and H. Verweij, *J. Am. Ceram. Soc*. 1997, **80**, 2175.
54. G. Lawes and G. Srinivasan, *J. Phys. D: Appl. Phys*. 2011, **44,** 243001 (22pp)

55. B. Ramachandran, A. Dixit, R. Naik, G. Lawes and M. S. Ramachandra Rao, *J. Appl. Phys.*, 2011, **110**, 104105.

Table 1: Magnetic Parameters at room temperature for the undoped and Gd/Fe doped nano $PbTiO_3$

Sample	Coercive field (Oe)	Saturation magnetization (emu/g)
$PbTiO_3$	257	0.013
$PbTiO_3$:Fe^{3+}(0.5%)	273	0.035
$PbTiO_3$:Gd^{3+}(0.5%)	265	0.020
$PbTiO_3$:Fe^{3+}(2%)	377	0.129
$PbTiO_3$: Gd^{3+}(0.5%)Fe^{3+}(2%)	346	0.074
$PbTiO_3$:Fe^{3+}(5%)	110	0.453
$PbTiO_3$: Gd^{3+}(0.5%)Fe^{3+}(5%)	105	0.385

Table 2: Electrical parameters at room temperature for the undoped and Gd/Fe doped nano $PbTiO_3$

Sample	Coercive field (kV/cm)	*P*s (μC/cm^2)	*P*r (μC/cm^2)
$PbTiO_3$	2.71	0.208	0.016
$PbTiO_3$:Fe^{3+}(0.5%)	5.06	0.334	0.063
$PbTiO_3$:Gd^{3+}(0.5%)	16.44	0.210	0.128
$PbTiO_3$:Fe^{3+}(2%)	16.56	0.572	0.413
$PbTiO_3$: Gd^{3+}(0.5%)Fe^{3+}(2%)	11.05	0.392	0.169
$PbTiO_3$:Fe^{3+}(5%)	16.26	0.513	0.353
$PbTiO_3$: Gd^{3+}(0.5%)Fe^{3+}(5%)	10.49	0.464	0.195

Figure Captions

Figure 1: Powder XRD pattern of (a) $PbTiO_3$, (b) $PbTiO_3$:Fe(0.5%), (c) $PbTiO_3$:Fe(2%) and (d) $PbTiO_3$:Fe(5%).

Figure 2: Powder XRD pattern of (a) $PbTiO_3$, (b) $PbTiO_3$:Gd(0.5%), (c) $PbTiO_3$:Gd(2%) and (d) $PbTiO_3$:Gd(5%). * indicates diffraction peaks corresponding to monoclinic $PbTi_3O_7$.

Figure 3: Powder XRD pattern of lead titanate samples doped with (a) Gd^{3+}(0.5%):Fe^{3+}(2%), (b) Gd^{3+}(0.5%):Fe^{3+}(5%) and (c) Gd^{3+}(2%):Fe^{3+}(2%).

Figure 4: XPS survey spectrum of (a) $PbTiO_3$, (b) $PbTiO_3$:Fe(5%), (c) $PbTiO_3$:Gd(0.5%), (d) $PbTiO_3$:Fe(5%)Gd(0.5%) and (e) comparative high resolution O1s core level XPS of all the above samples.

Figure 5: TEM image of a) $PbTiO_3$, c) $PbTiO_3$:Fe(5%), corresponding EDX of b) $PbTiO_3$, d) $PbTiO_3$:Fe(5%) and HRTEM image of e) $PbTiO_3$ and f) $PbTiO_3$:Fe(5%) samples with inset showing corresponding SAED pattern.

Figure 6: Magnetization vs. Field (*M-H*) curves for undoped and Fe/Gd doped $PbTiO_3$ samples

Figure 7: Magnetization vs. temperature (*M-T*) curves for $PbTiO_3$:Fe(2%), $PbTiO_3$:Fe(5%) and $PbTiO_3$:Fe(5%):Gd(0.5%) samples at magnetic field strength of 500Oe. The insets show *M-H* curves at 50 and 300K for the three samples.

Figure 8: (a) Polarization-electric field hysteresis loops and (b) Leakage current as a function of applied electric field for undoped and Gd/Fe doped $PbTiO_3$ nanoparticles.

Figure 9: Magnetic field dependence of the capacitive response for (a) $PbTiO_3$:Fe(5%):Gd(0.5%) and (b) $PbTiO_3$:Fe(5%) samples.

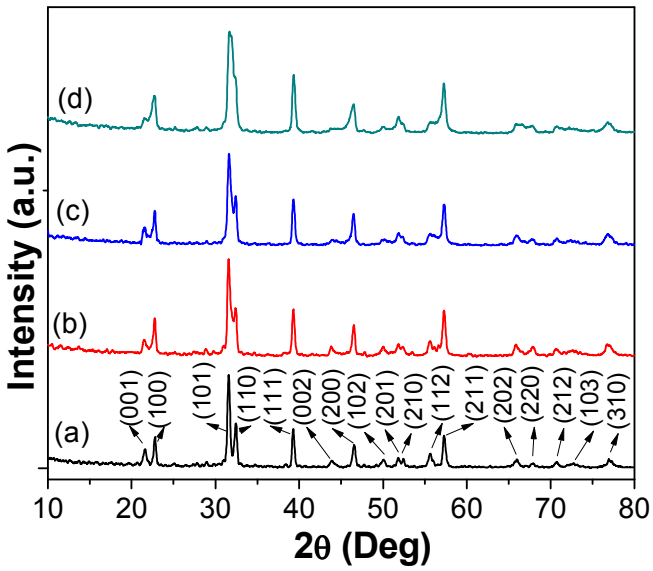

Figure 1: Powder XRD pattern of (a) $PbTiO_3$, (b) $PbTiO_3$:Fe(0.5%), (c) $PbTiO_3$:Fe(2%) and (d) $PbTiO_3$:Fe(5%).

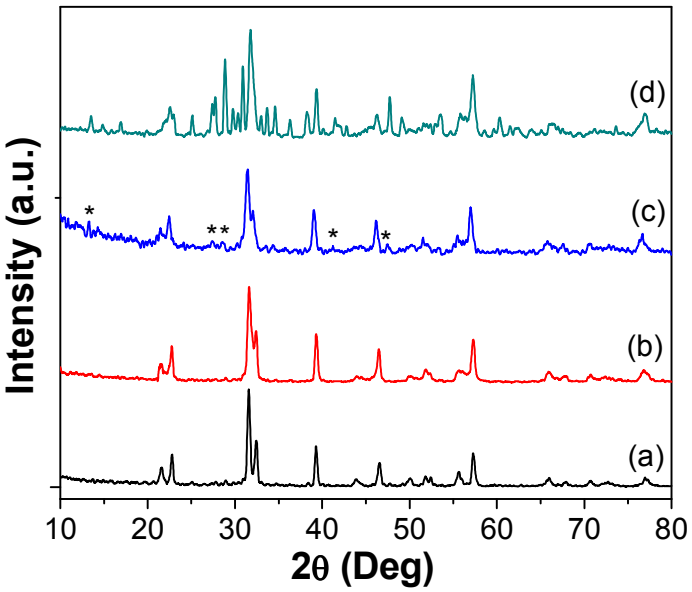

Figure 2: Powder XRD pattern of (a) $PbTiO_3$, (b) $PbTiO_3$:Gd(0.5%), (c) $PbTiO_3$:Gd(2%) and (d) $PbTiO_3$:Gd(5%). * indicates diffraction peaks corresponding to monoclinic $PbTi_3O_7$.

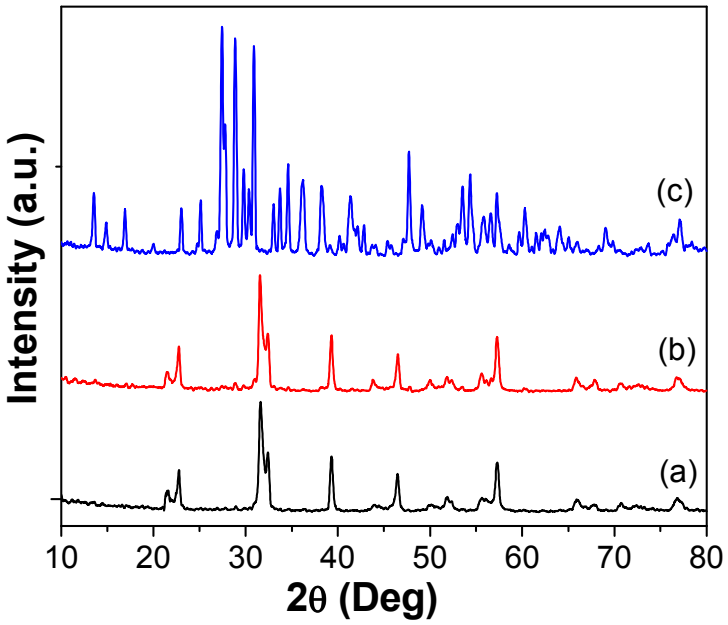

Figure 3: Powder XRD pattern of lead titanate samples doped with (a) Gd^{3+}(0.5%):Fe^{3+}(2%), (b) Gd^{3+}(0.5%):Fe^{3+}(5%) and (c) Gd^{3+}(2%):Fe^{3+}(2%).

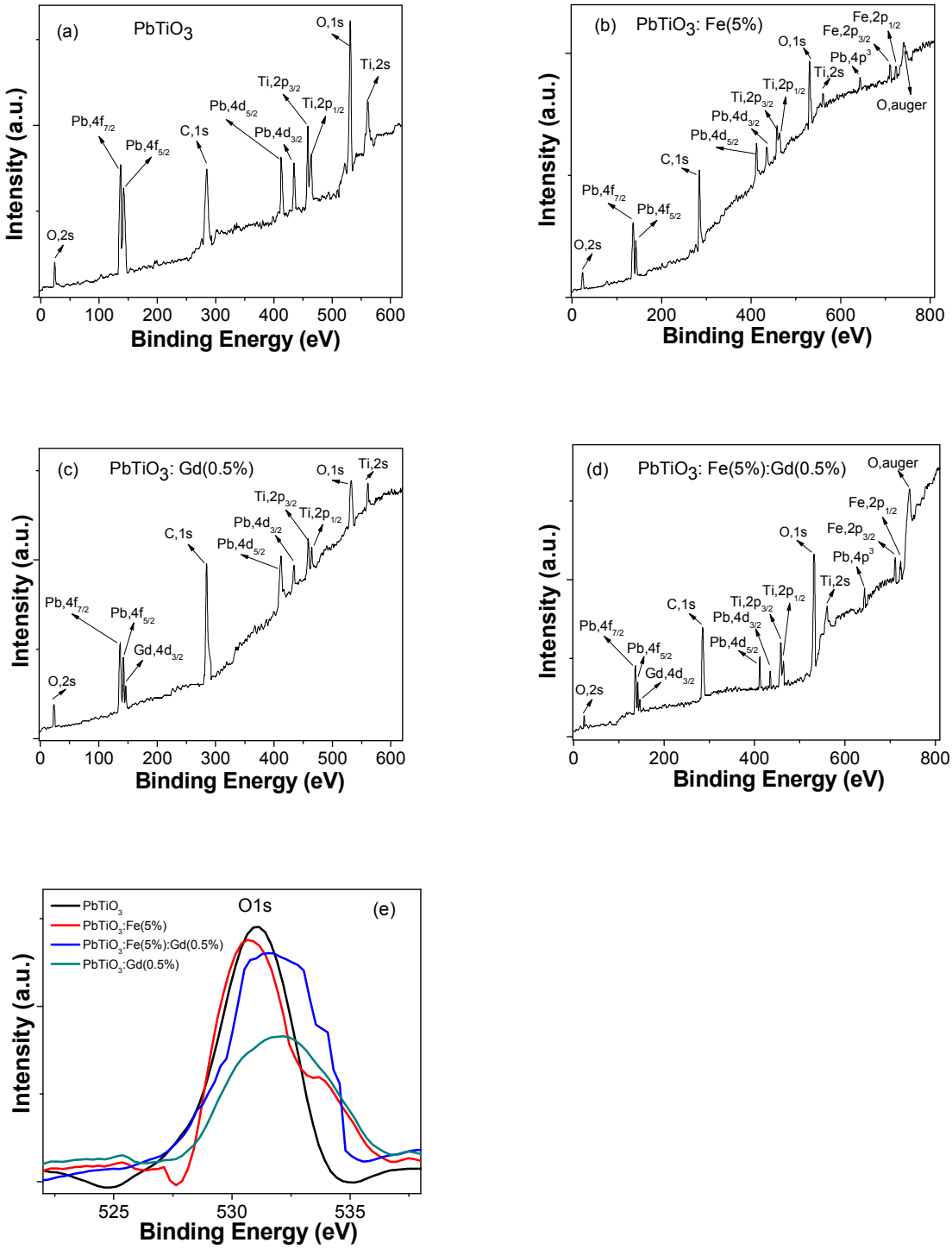

Figure 4: XPS survey spectrum of (a) $PbTiO_3$, (b) $PbTiO_3$:Fe(5%), (c) $PbTiO_3$:Gd(0.5%), (d) $PbTiO_3$:Fe(5%)Gd(0.5%) and (e) comparative high resolution O1s core level XPS of all the above samples.

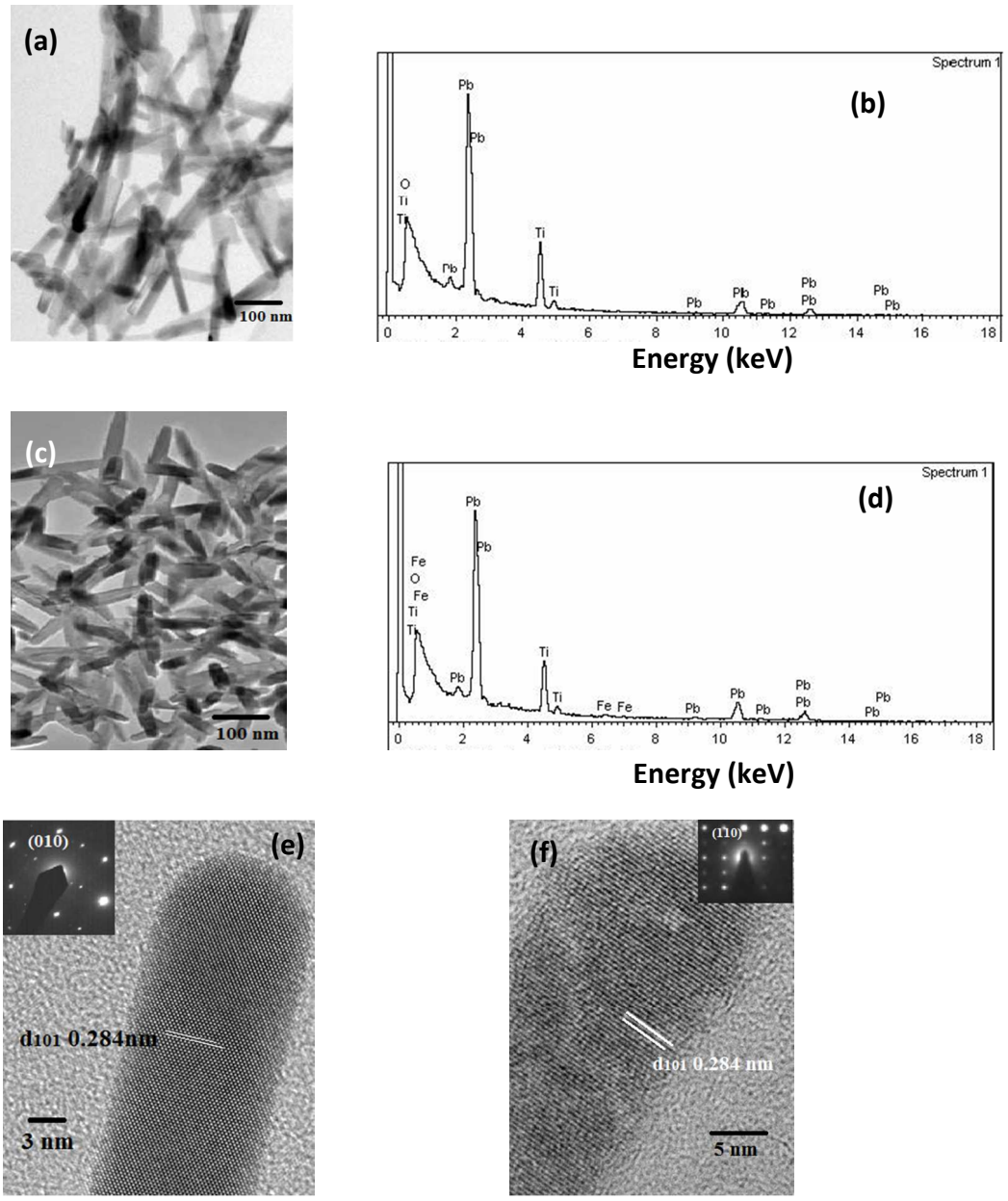

Figure 5: TEM image of a) $PbTiO_3$, c) $PbTiO_3$:Fe(5%), corresponding EDX of b) $PbTiO_3$, d) $PbTiO_3$:Fe(5%) and HRTEM image of e) $PbTiO_3$ and f) $PbTiO_3$:Fe(5%) samples with inset showing corresponding SAED pattern.

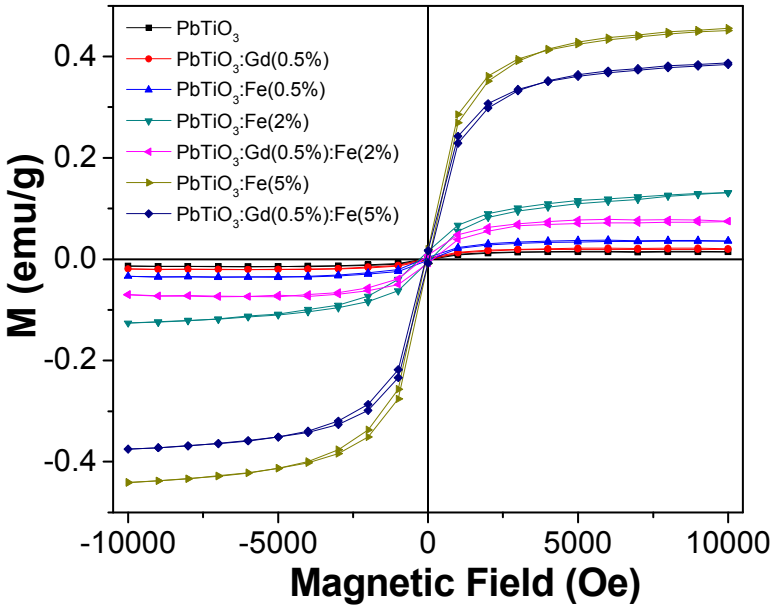

Figure 6: Magnetization vs. Field (*M-H*) curves for undoped and Fe/Gd doped $PbTiO_3$ samples at room temperature (300K)

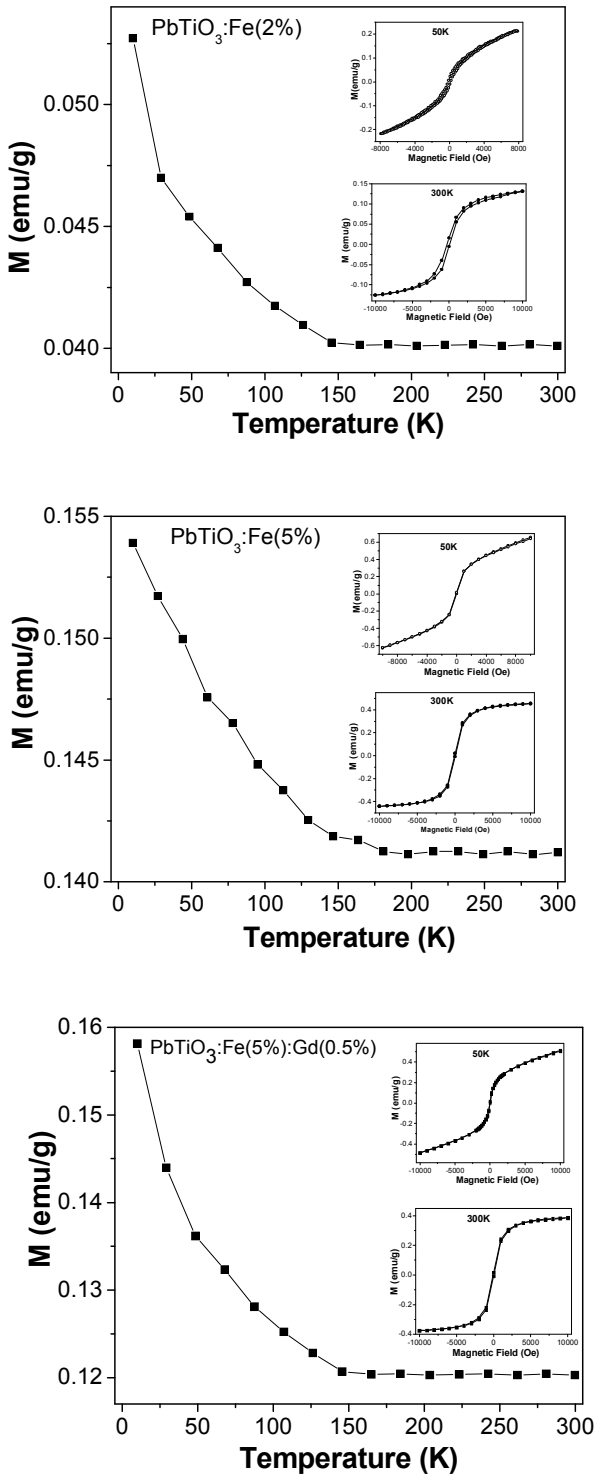

Figure 7: Magnetization vs. temperature (*M-T*) curves for $PbTiO_3$:Fe(2%), $PbTiO_3$:Fe(5%) and $PbTiO_3$:Fe(5%):Gd(0.5%) samples at magnetic field strength of 500Oe. The insets show *M-H* curves at 50 and 300K for the three samples.

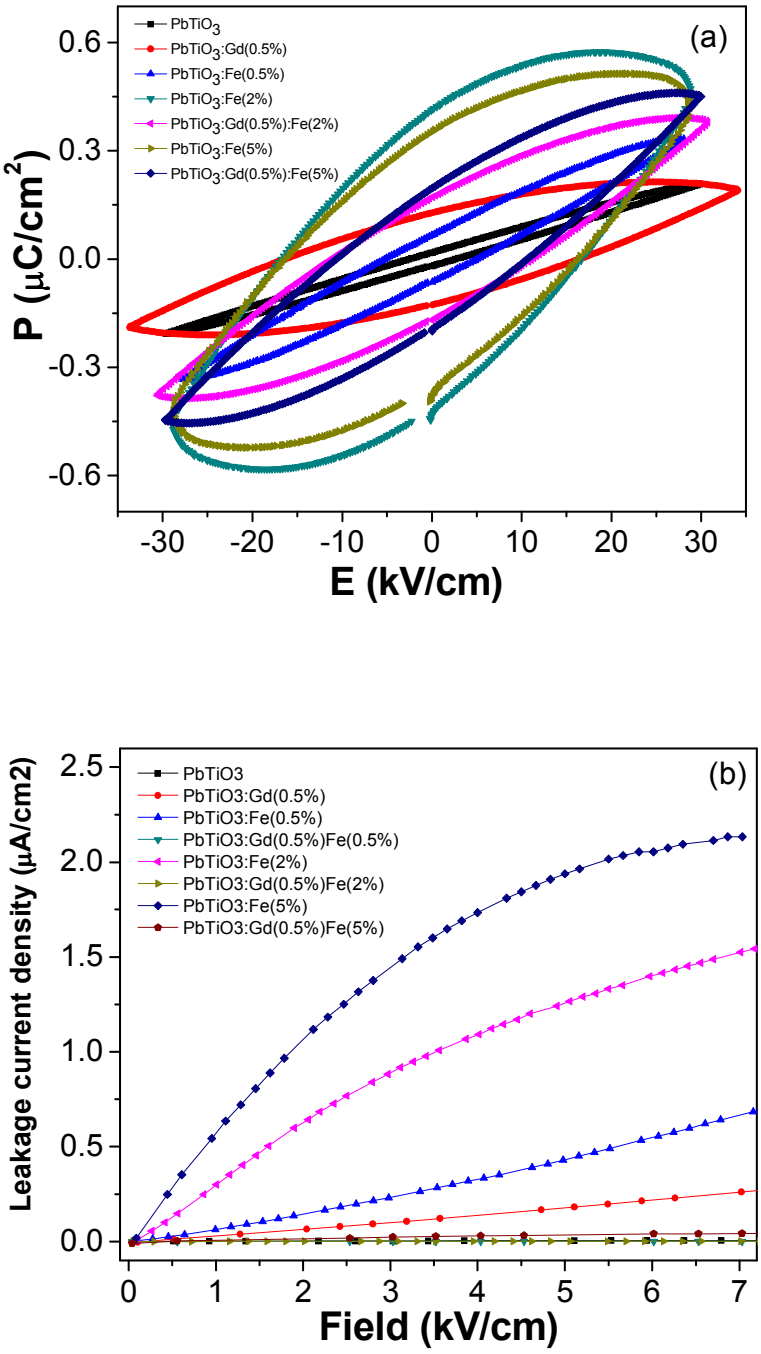

Figure 8: (a) Polarization-electric field hysteresis loops and (b) Leakage current as a function of applied electric field for undoped and Gd/Fe doped $PbTiO_3$ nanoparticles.

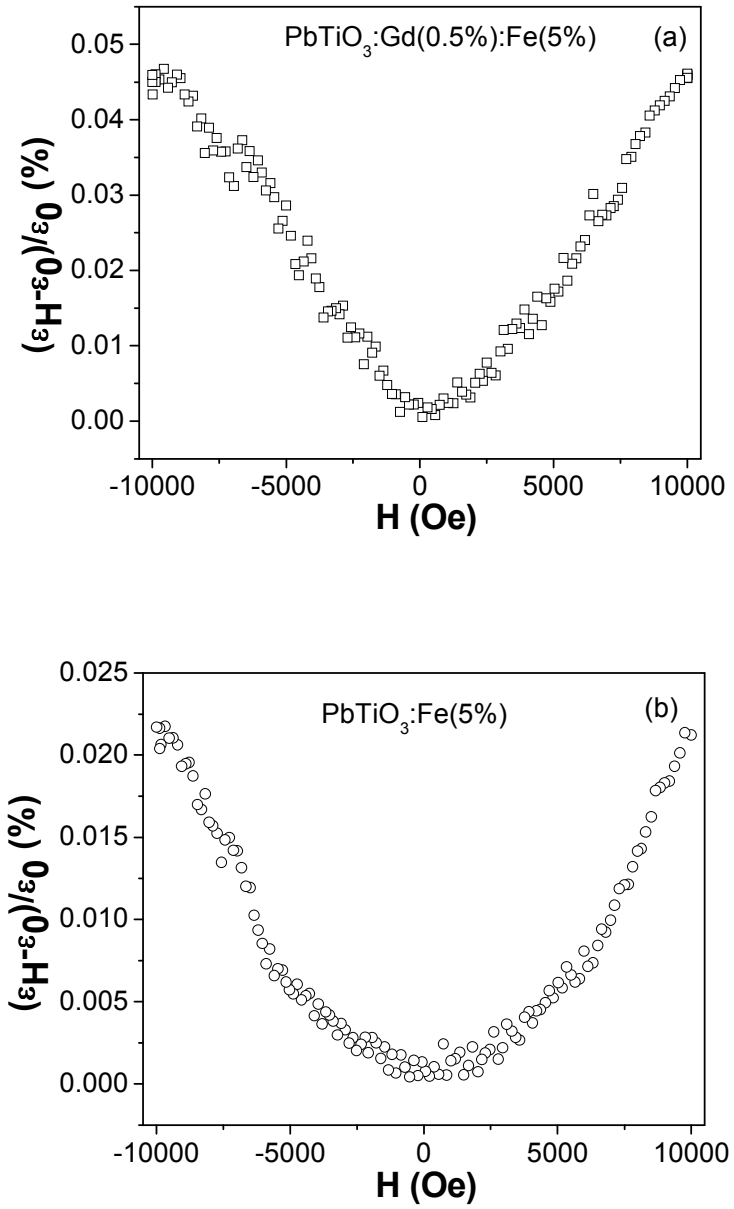

Figure 9: Magnetic field dependence of the capacitive response for (a) $PbTiO_3$:Fe(5%):Gd(0.5%) and (b) $PbTiO_3$:Fe(5%) samples.